Eur. Phys. J. B **60**, 15–27 (2007)
DOI: 10.1140/epjb/e2007-00320-3

THE EUROPEAN PHYSICAL JOURNAL B

Transient domain wall displacement under spin-polarized current pulses

A. Thiaville[1,a], Y. Nakatani[2], F. Piéchon[1], J. Miltat[1], and T. Ono[3]

[1] CNRS, Laboratoire de Physique des Solides, UMR 8502, 91405 Orsay, France
and
Univ. Paris-Sud, Bâtiment 510, 91405 Orsay, France
[2] Department of Computer Science, Univ. of Electrocommunications, Chofu, 182-8585 Tokyo, Japan
[3] Institute for Chemical Research, Kyoto Univ., Uji, 611-0011 Kyoto, Japan

Received 3 July 2007
Published online 23 November 2007 –

Abstract. This paper investigates the non steady-state displacement of magnetic domain walls in a nanostrip submitted to a time-dependent spin-polarized current flowing along the nanostrip. First, numerical micromagnetic simulations show that a domain wall can move under application of a current pulse, and that the displacement resulting from a conversion of the domain wall structure is quantized. The numerical findings are subsequently explained in the framework of simplified analytic models, namely the 1D model and the point-core vortex model. We then introduce the concept of an angle linked to the magnetization of a general domain wall, and show that it allows understanding the transient phenomena quite generally. Simple analytic formulas are derived and compared to experiments. For this, charts are given for the key parameters of the domain wall mechanics, as obtained from numerical micromagnetic simulations. We finally discuss the limitations of this work, by looking at the influence of temperature elevation under current, presence of a non-adiabatic term, and of disorder.

PACS. 72.25.-b Spin polarized transport – 85.75.-d Magnetoelectronics; spintronics – 75.75.+a Magnetic properties of nanostructures – 75.60.Ch Domain walls and domain structure

1 Introduction

The dynamics of magnetic domain walls (DW) under a current flowing inside the magnetic material is presently a very active research topic. The initial work by Berger [1,2] has uncovered several mechanisms for this interaction, the most investigated nowadays being the spin-transfer torque [2], where the angular momentum carried by the spin-polarized current is delivered to the DW magnetic moments upon DW crossing by conduction electrons. The progress in micro- and nanofabrication techniques now allows confining, preparing and manipulating the DW in suitably designed structures [3–5]. This is ideal for the experimental study of this effect.

Following several experimental observations of the DW displacement and velocity by spin-polarized current [5–8], application of the phenomenon to new magnetic devices is now envisioned. For such applications, fast displacement of DWs is required, implying short current pulses. Experiments are also mostly performed with pulsed currents, because of the high current densities required that could destroy the samples in dc regime. In some cases, a DW displacement proportional to pulse duration has been observed [7,9], testifying for the existence of DW velocity under current. In other cases, however, the DW displacement was found to disappear after several pulses, this being related to a DW structural transformation [8]. In one case even, a very large apparent DW displacement that did not depend on pulse duration (ns regime) was observed [10]. Thus, the theoretical investigation of the DW displacement under spin-polarized current pulses appears to be necessary. Past micromagnetic modelling of the current-driven DW dynamics has been mainly devoted to the steady-state regime. In such a situation, general micromagnetic relations can be applied that greatly simplify the analysis. The main outcome of these studies was that, in order to obtain a steady state DW motion under zero field, a second torque term was required. Specifically, the Landau-Lifschitz-Gilbert (LLG) equation of micromagnetics that rules the magnetization dynamics is proposed to be modified to

$$\dot{\boldsymbol{m}} = \gamma_0 \boldsymbol{H}_{\text{eff}} \times \boldsymbol{m} + \alpha \boldsymbol{m} \times \dot{\boldsymbol{m}} - (\boldsymbol{u} \cdot \boldsymbol{\nabla})\, \boldsymbol{m} + \beta \boldsymbol{m} \times [(\boldsymbol{u} \cdot \boldsymbol{\nabla})\, \boldsymbol{m}] \,. \quad (1)$$

In this equation, $\boldsymbol{m}$ is the local (position and time dependent) magnetization orientation ($|\boldsymbol{m}| = 1$), the overdot denotes time derivation, $\gamma_0 = \mu_0 |\gamma|$ is the gyromagnetic ratio, $\boldsymbol{H}_{\text{eff}}$ the effective field of micromagnetics and

[a] e-mail: thiaville@lps.u-psud.fr

α the Gilbert damping constant [11]. The current effect is expressed by the so-called adiabatic term, where $\boldsymbol{u}$ is a velocity proportional to the spin current in direction and magnitude, and a second, called non-adiabatic, term whose relative magnitude is given by the dimensionless factor β [12,13]. Numerically, a current density $J = 1 \times 10^{12}$ A/m^2 corresponds to $u = 70$ m/s for a 100% current polarization P, or to 50 m/s for a more realistic $P = 0.7$. This allows converting all values of u given in the following into current densities.

Two different conceptions of the introduction of the current-induced torque exist. If damping is considered to act on the current-induced torque term in the same way as on the effective field term, then non-adiabaticity is measured by comparing β to 0. If, on the other hand, it is assumed that no damping can apply to the current-driven torque term (because there is no energy from which it derives [14,15]), then $\beta - \alpha$ is a measure of the non-adiabaticity.

In this paper, we look at the case $\beta = 0$ in detail, for a spatially uniform but time-dependent current (shaped as a step or pulse) and in absence of an applied field. We show that a transient DW displacement appears upon current application, that can be as large as several micrometers. This displacement is shown to exist both at current onset (current step situation) and after a current pulse has terminated. We relate this transient displacement to a transformation of the DW structure, shown to be measured by the variation of an "angle" of the DW, which we define in full generality. Our study starts by micromagnetic numerical simulations (Sect. 2), then uses analytical models (Sect. 3) before introducing general micromagnetic concepts that are useful to study the various experimental configurations (Sect. 4). Quantitative estimations of the DW transient displacement are given, and compared to experiments. In order to do such comparisons easily, we construct a series of charts displaying the main quantities that characterize the DW dynamics, as discussed in this paper, as a function of nanostrip width and thickness.

2 Representative micromagnetic simulation results

We start by describing the results of micromagnetic numerical simulations of transient effects during a current step or pulse. These results were obtained using a programme described previously [12]. Briefly stated, it uses a 2D mesh with cells of size $a \times a \times h$, where h is the nanostrip thickness and a the mesh size (4 nm here). A moving calculation region, extended 2 μm along the nanostrip, is used for calculating DW structure and dynamics [12]. The Œrsted field created by the current is not included in the calculations, unless otherwise specified, as it hardly affects results. Temperature effects caused by resistive heating of the sample under current are also not included. Temperature rise is indeed extremely dependent on sample architecture, and minimal temperature rises have been measured in some cases. Material parameters used in these calculations were those typical for permalloy, namely exchange constant $A = 10^{11}$ J/m, anisotropy $K = 0$, magnetization density $M_\mathrm{s} = 8 \times 10^5$ A/m, gyromagnetic ratio $\gamma_0 = 2.21 \times 10^5$ m/(As), and damping factor $\alpha = 0.01$, or 0.02 as adapted to patterned thin films [16].

2.1 Transverse wall in a 120 × 5 nm^2 nanostrip

This structure (see images in Sect. 4.4) was investigated in one early experiment [6], and the transverse wall is clearly stable at these small nanostrip dimensions [17,18].

2.1.1 Current step

Consider first the effect of a current applied instantaneously at time $t = 0$. We first look at currents such that u is below the threshold value u_c ($\simeq$600 m/s here) for continuous DW motion [19]. Figure 1a shows that the DW starts with a initial velocity $v_0 = u$, and that this velocity drops to 0 over a duration of the order of a nanosecond. In fact, DW velocity is proportional to the equivalent velocity u, with a systematic deviation apparent at large u values. The accumulated DW displacement q during the transient period is also proportional to u, with again some deviation at large u, so that we write

$$[q]_0^\infty \approx u\tau, \tag{2}$$

where τ is the characteristic time of the DW structure evolution towards its stable state under current (throughout the paper, square brackets will be used to denote the change of the variable between the 2 times considered). This time can be evaluated by fitting the curves $v(t)$, $q(t)$ with exponentials. Figure 1 also shows the time evolution of the angle of the wall magnetization, called Φ. This angle will be defined in Section 4, but for the moment we can use the physical image of the angle, with respect to the nanostrip plane, of the DW transverse moment. The angle shows an evolution similar to that of the DW displacement q, with a similar relaxation time.

These calculations pertain to an infinitely fast pulse risetime, so that it is interesting to know how a finite, more realistic, risetime would affect them. Figure 1c shows that, even if the dynamics is affected, the wall displacement q and angle Φ converge to the same values. Thus, to a given height of the current step we can associate, in equilibrium, a change of wall angle and a change of wall position.

If the current is increased so that $u > u_\mathrm{c}$, continuous precession of the wall angle sets in, together with wall displacement, as is well known [19,20]. Figure 2 displays the result for $u = 620$ m/s, just above u_c. The angle Φ shows a straicase-like decrease, where the plateaus are close to $\Phi = n\pi$. The wall position shows a similar behaviour. We have shown previously that the transverse wall conversion occurs through the injection and motion of an antivortex (AV, see image in Sect. 4.4) across the strip width [19]. During that phase the wall is set into motion.

The DW displacement for each step amounts to $[q] \approx 2600$ nm for $[\Phi] = \pi$. Comparing with the results above, we

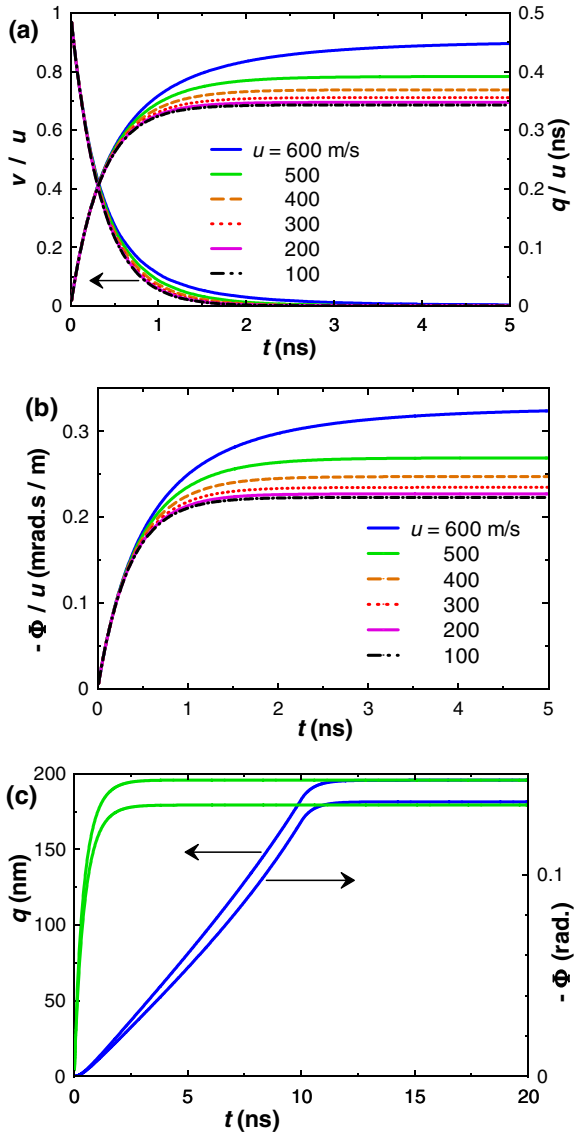

Fig. 1. (Color online) Dynamics of a transverse wall in a 120×5 nm^2 nanostrip submitted at time $t = 0$ to a spin-polarized current, for various values of the equivalent velocity u. (a) For a zero risetime, both the scaled velocity and DW displacement relax exponentially towards their final value. (b) Plot of the time variation of the DW magnetization angle Φ, also scaled to u, still for zero risetime. (c) The comparison, in the case $u = 500$ m/s, of the evolutions for risetimes of 0 and 10 ns, shows identical final values (a better agreement results if the mesh size is decreased).

see that they all correspond to a proportionality $[q] / [\Phi] \approx 1500$ nm/rad.

2.1.2 Current pulse

In experiments, current pulses of finite duration are applied, so that it is important to know what happens after a pulse. A trapezoidal pulse is considered here, similar to the

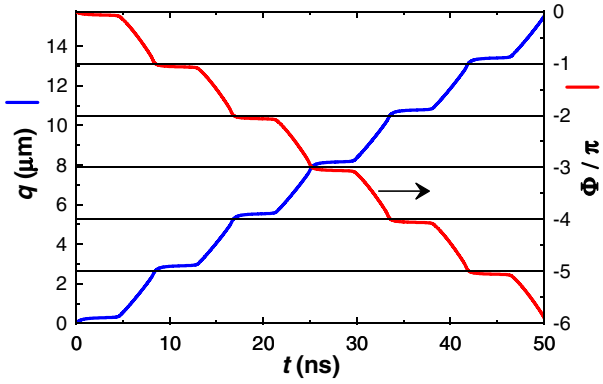

Fig. 2. (Color online) Dynamics of a transverse wall in a 120×5 nm^2 nanostrip submitted at time $t = 0$ to a spin-polarized current $u = 620$ m/s above the critical value. DW position q increases in a step-like way, the DW magnetization angle changing by π at each step.

shape used for the ultra-fast experiment quoted above [10], with risetime of 1/3 ns, plateau 1 ns and falltime 2/3 ns.

Figure 3 shows the evolution of DW displacement q and angle Φ for four values of the peak current. For low values, q and Φ reach some maximum value during the pulse and return to zero after it has terminated. For high enough currents, however, a large after-pulse DW displacement appears $[q] \approx 2600$ nm, and the wall angle has increased by π. These are the same values as seen previously for a current step. For this pulse shape and duration, DW magnetization reversal is seen for $u > 1200$ m/s, a value twice as large as u_c. Longer pulse durations give values closer to u_c (not shown). This may be understood from the transverse velocity of the AV (itself a function of applied current) that results into a minimum time for DW structure conversion. At $u = 1200$ m/s, the calculation movie shows that the AV has just passed half of the strip width as the pulse ends, so that it moves slowly to the other edge of the strip after pulse termination (Fig. 3).

2.2 Vortex wall in a 240 × 10 nm^2 nanostrip

The previous results pertain to the simplest DW structure, the transverse wall (TW). However, vortex walls (VW, see image in Sect. 4.4) that are stable in thicker and wider nanostrips, easier to fabricate, are in most instances observed experimentally. The dimensions considered here are, for example, those of the first direct observation by magnetic force microscopy of DW displacement and velocity under current [7].

For a current step (Fig. 4), the conclusions are similar to those reached for the TW, but with very different numbers. The time constant τ is now much longer ($\sim$8 ns, compared to 0.5 ns in Fig. 1), and the critical current equivalent velocity much lower ($\sim$130 m/s). Large quantitative differences are also seen above this critical value. First, the angle Φ rises to $\pi/2$ instead of π, and moreover the DW stops after this conversion. Movies (and the plot of the

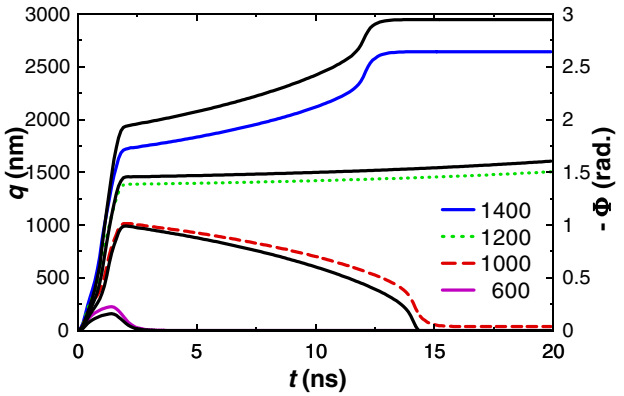

Fig. 3. (Color online) Dynamics of a transverse wall in a 120×5 nm^2 nanostrip submitted at time $t = 0$ to a spin-polarized current pulse (duration 2 ns, rise and fall times of 1/3 and 2/3 ns, respectively), for various values of the current equivalent velocity u. DW position is shown in color with broken lines, and the corresponding negative of DW magnetization angle in black, continuous lines. More precise angle values (closer to 0 or π after the pulse) are obtained with a smaller calculation mesh size.

maximum perpendicular component, m_z, of the magnetization) show that the conversion occurs from VW to TW. The displacement $[q]$ resulting from this '$\pi/2$ conversion' is ∼1600 nm. At larger currents, this TW sets in continuous motion, similarly to the previous case (Fig. 4c). Depending on the value of current, however, the DW structure continuous conversion appears to be realised by V only, or V and AV in alternance.

Current pulses give similar values for the increments $[q]$ and $[\Phi]$. Such calculations were repeated for other dimensions, with similar results. Thus, a more general understanding of these phenomena seems possible. This is the object of the next sections.

3 Analytical models

We look for as simple as possible an explanation of the features revealed by numerical simulations. For this, several models are considered, with increasing generality. The most employed model is the 1D model, designed for the TW [20–23]. The point core model for a VW is then considered and we show that, despite the different energetics of these two models, strikingly similar conclusions are obtained.

3.1 1D model

The 1D model, adapted from the initial calculation of the 1D Bloch wall and of its dynamics to the nanowire- nanostrip geometry [21,23,24] considers just two dynamic variables for a DW, namely its x position q along the nanostrip, and the angle of the DW magnetization Φ. A possible additional parameter is the wall width parameter Δ. The

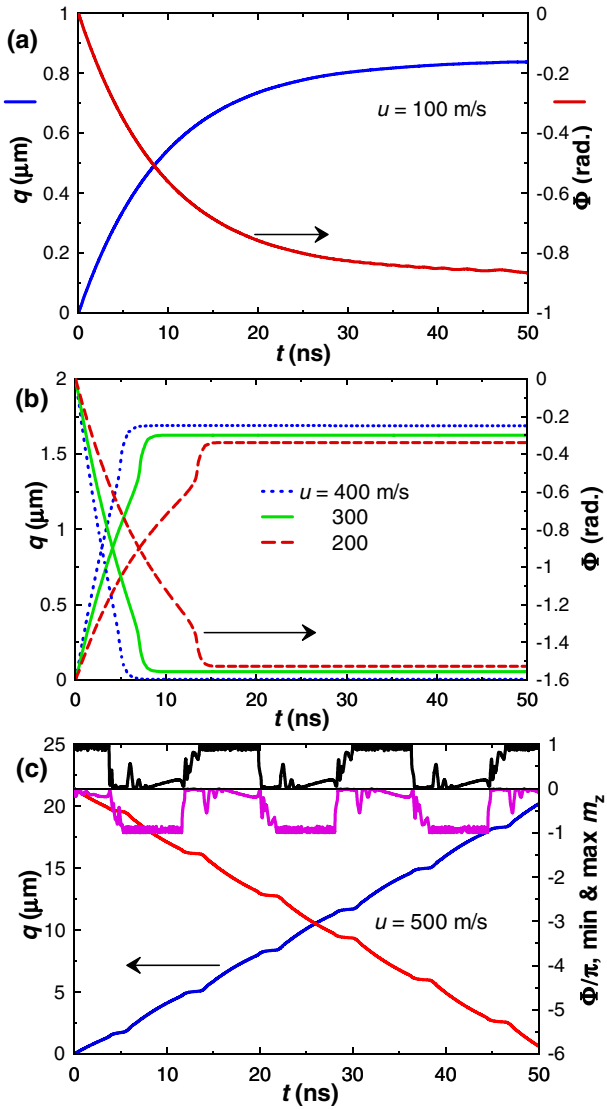

Fig. 4. (Color online) Dynamics of a vortex wall in a 240×10 nm^2 nanostrip submitted at time $t = 0$ to a spin-polarized current, for various values of the equivalent velocity u. (a) For low current, the DW relaxes towards its equilibrium structure, with a large time constant and undergoes a sizeable displacement. (b) For intermediate currents, the VW transforms to a TW (corresponding to the $\pi/2$ variation of the wall angle), and displaces by the corresponding quantity. (c) Still larger currents cause the instability of the TW itself, that leads to continuous DW motion with Φ precession. In addition, the maximum and minimum values of the local perpendicular magnetization component are shown (the noise in the vicinity of ± 1 is due to the calculation mesh size).

dynamic equation initially written for Δ [21] was of the relaxation type, with a very short time constant [23]. Recent work [25] has however shown that a variable conjugated to Δ exists, namely an asymmetry of the DW profile. Nevertheless, in the approximation where the time constant for Δ is shorter than the timescales of all other phenomena, Δ simply behaves as a 'slave' function of the angle Φ.

The 1D model dynamic equations including field and non-adiabatic term read [12]

$$\dot{\Phi} + \alpha \frac{\dot{q}}{\Delta} = \gamma_0 H_\mathrm{a} + \beta \frac{u}{\Delta} \tag{3}$$

$$\frac{\dot{q}}{\Delta} - \alpha \dot{\Phi} = \gamma_0 H_K \sin\Phi\cos\Phi + \frac{u}{\Delta} \tag{4}$$

where H_a is the applied field along the strip axis (x), H_K is the effective transverse anisotropy field and $u(t)$ is the time-dependent spin-transfer torque due to the current pulse or step. As we consider here the case of no applied field and action of a sole adiabatic torque, we have from (3) by time integration

$$[q] = -\frac{1}{\alpha}\int_{\Phi_\mathrm{i}}^{\Phi_\mathrm{f}} \Delta(\Phi)\, d\Phi. \tag{5}$$

DW displacement is therefore directly linked to the change of the angle Φ, independently of the time variation of the spin-polarized current. The dynamics of Φ is obtained from (4) where the wall position has been eliminated, as

$$\dot{\Phi} = -\frac{\alpha}{1+\alpha^2}\left[\frac{u}{\Delta} + \gamma_0 H_K \sin\Phi\cos\Phi\right]. \tag{6}$$

For small angles, the evolution is exponential, with a time constant

$$\tau_\mathrm{1D} = \frac{1+\alpha^2}{\alpha\gamma_0 H_K}. \tag{7}$$

The 1D model also allows evaluating the change of Φ under current application (current step case). Requiring $\dot{\Phi} = 0$ in (6) gives the value Φ^* towards which $\Phi(t)$ converges under constant current as

$$\Delta(\Phi^*)\sin 2\Phi^* = -\frac{2u}{\gamma_0 H_K}. \tag{8}$$

For small u, thus small Φ, $[\Phi] = \Phi^* = -u/(\gamma_0 H_K \Delta_0)$ so that the change of DW position under current application is

$$[q] = \frac{u}{\alpha\gamma_0 H_K} = \left(1+\alpha^2\right)\frac{u}{\tau_{1D}}$$

$$[q] = -\frac{\Delta_0}{\alpha}[\Phi]. \tag{9}$$

Extending these relations to the non linear regime is possible. The variation of Δ with Φ in the standard 1D model with a transverse anisotropy of degree 2 is [23]

$$\Delta(\Phi) = \frac{\Delta_0}{\sqrt{1+\kappa\sin^2\Phi}}, \tag{10}$$

where Δ_0 is the DW width parameter at rest, and

$$\kappa = K/K_0 \tag{11}$$

is the ratio of the effective transverse to axial anisotropies. These anisotropies derive mainly from the magnetostatic term, so that κ is essentially proportional to the aspect ratio of the nanostrip cross-section [23,24]. Defining the linear Walker velocity as

$$v_\mathrm{W} = \gamma_0 \Delta_0 H_K/2 \tag{12}$$

and the normalized velocity $U = u/v_\mathrm{W}$, the wall angle in the non linear regime can be expressed as

$$\cos 2\Phi^* = \frac{\kappa U^2}{4} + \sqrt{1 - U^2\left(1+\frac{\kappa}{2}\right) + \frac{U^4\kappa^2}{16}}. \tag{13}$$

The solution exists only when U is smaller than a value

$$U_\mathrm{max} = 2\left(\sqrt{1+\kappa} - 1\right)/\kappa. \tag{14}$$

The associated DW displacement is now written as

$$[q] = -\frac{\Delta_0}{\alpha} g(\Phi^*) \tag{15}$$

where g is an elliptic function defined by

$$dg/d\Phi = 1/\sqrt{1+\kappa\sin^2\Phi}. \tag{16}$$

These relations are plotted in Figure 5.

The effective parameters to be used for the sample dimensions considered here have been determined before [23]: $\Delta_0 = \Delta_x = 37.7$ nm, $H_\mathrm{K} = 2K/\mu_0 M_\mathrm{s} = 545$ kA/m and $\kappa = 11.9$. From these values one computes $v_\mathrm{W} = 2270$ m/s, $u_\mathrm{max} = 988$ m/s and $\tau_\mathrm{1D} = 0.42$ ns for $\alpha = 0.02$. Note that u_max is of the same order as the numerical value (600 m/s), but sizeably larger. Such a difference is however not a surprise: the 1D model is not quantitatively correct for such a wide nanostrip (the width is 24 times the exchange length). Another proof of this quantitative shortcoming is provided by the different values of the domain wall width: $\Delta_x = 37.7$ nm is derived from the width-averaged longitudinal component m_x profile, $\Delta_\mathrm{t} = 31.3$ nm from the transverse component (m_y here) and $\Delta_\mathrm{T} = 30.7$ nm is the calculated Thiele width.

For small u, the 1D model result is $[q]/\Phi^* = \Delta_0/\alpha = 1885$ nm/rad, close to the value numerically obtained (1500 nm/rad). For large angles one finds, for a TW magnetization reversal where $\Phi^* = \pi$, $[q] = \Delta_0 g(\pi)/\alpha = 2831$ nm, again close to the numerical value (2600 nm).

Altogether, we see that the 1D model can provide a fair understanding of the results found for the TW with dimensions such as considered above. Quantitative discrepancies are already uncovered at this lateral size that lies within the smallest that are currently fabricated.

3.2 Point core vortex model

For a VW, the domain wall magnetization angle is not intuitive, and the prominent feature of the DW structure is the vortex core. The point core vortex model, in its simplest form, replaces the dynamic variable Φ by the lateral position y_c of this core. The lateral motion of this core realizes the domain wall transformation. The dynamics of the vortex wall with this internal degree of freedom is

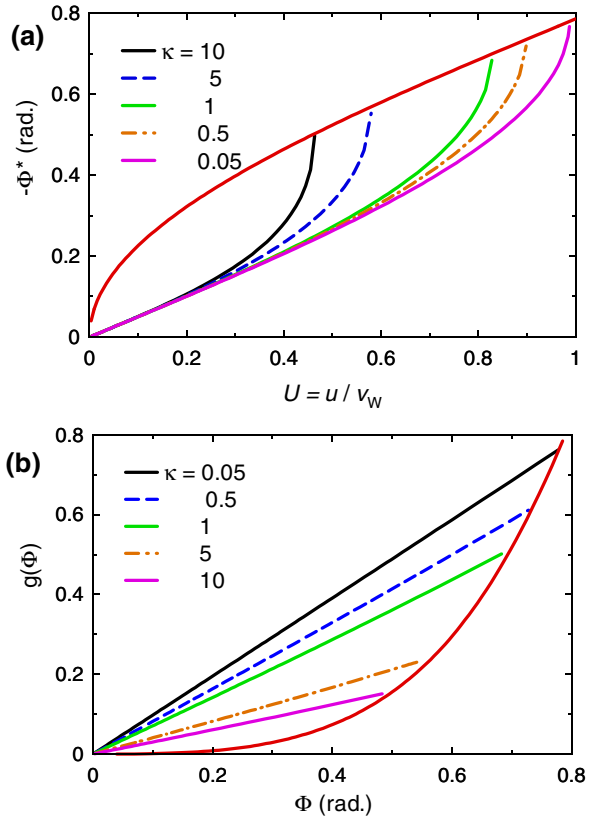

Fig. 5. (Color online) Non linear solution of the 1D model with slave DW width for a TW submitted to a spin-polarized current represented by the equivalent velocity u. The parameter κ is the ratio of the transverse to axial effective anisotropies, and $v_{\rm W}$ the Walker velocity (see text). (a) DW magnetization angle Φ^* as function of reduced current, for several values of κ (note that the Walker velocity depends also on that parameter). The continuous green line draws the locus of the maxima (in the constant width model, *i.e.* $\kappa = 0$, this value is $\pi/4$). (b) The function $g(\Phi)$ giving the scale of the DW displacement under change of wall angle. The continuous red curves draw the loci of the maxima.

obtained from the Thiele equation, an integrated form of the LLG equation [26,27]. This model was recently applied successfully to several cases [28–30].

Here, whereas DW motion along the nanostrip may be stationary, the core transverse motion cannot, because of the finite width of the nanostrip. Nevertheless, it is conceivable to extend the Thiele equation by considering at every time the DW motion to be a mere solid translation of the structure. This neglects the deformations of the structure due to the presence of the lateral boundaries and to the change of velocity. The former will be important when the core is close to the boundaries, but as the core starts from the strip center we may neglect them. The latter effect is just the DW mass [31]. Several calculations of the mass associated to vortex dynamics have been published [32,33], and in the VW geometry the mass can be related to the other parameters that we consider in this paper [34]. This term is usually neglected when analysing experiments, as the vortex velocity is not very large [29].

In the presence of a spin-polarized current, the Thiele equation is modified to [12]

$$\boldsymbol{F} + \boldsymbol{G} \times (\boldsymbol{v} - \boldsymbol{u}) - \overleftrightarrow{D}\,(\alpha \boldsymbol{v} - \beta \boldsymbol{u}) = \boldsymbol{0}, \qquad (17)$$

where we have changed the sign of the dissipation matrix D from the original definition [26] so that D is positive. In this equation, $\boldsymbol{v} = d\boldsymbol{X}/dt$ is the vortex wall 2D velocity where $\boldsymbol{X} = (q, y_{\rm c})$ is the vector position of the vortex core, and $\boldsymbol{u}$ is the velocity equivalent to the spin-polarized current. The gyrovector $\boldsymbol{G}$ has only a component G on the z axis perpendicular to the strip plane, with a 'quantized' value [26] $G = (\mu_0 M_{\rm s}/\gamma_0)\, 2\pi h p$, where $p = \pm 1$ is the polarity of the vortex core (the direction of its perpendicular magnetization at the center). The matrix $\overleftrightarrow{D}$ is the dissipation matrix, and finally $\boldsymbol{F} = -\partial E/\partial \boldsymbol{X}$ is the force applied on the vortex core. In the absence of an applied field, the total energy can only depend on the core lateral position $y_{\rm c}$, so $\boldsymbol{F}$ has only a y component that we linearize in the vicinity of the the strip center $F_y = -\kappa y_{\rm c} + ...$ Specializing again to the $\beta = 0$ case, we obtain for a general dissipation matrix [35]

$$-G\dot{y}_{\rm c} - \alpha D_{xx}\dot{q} - \alpha D_{xy}\dot{y}_{\rm c} = 0, \qquad (18)$$

$$-\kappa y_{\rm c} + G\,(\dot{q} - u) - \alpha D_{yy}\dot{y}_{\rm c} - \alpha D_{xy}\dot{q} = 0. \qquad (19)$$

The first equation (18) means that VW motion is linked to the lateral motion of the vortex core. From (19) one sees that the latter is exponential, with a time constant

$$\tau_{\rm VW} = \frac{G^2 + \alpha^2\left(D_{xx}D_{yy} - D_{xy}^2\right)}{\alpha D_{xx}\kappa} \approx \frac{G^2}{\alpha D_{xx}\kappa}. \qquad (20)$$

As G/h is quantized, and D/h does not vary significantly, $\tau_{\rm VW}$ depends essentially on κ/h, *i.e.* on the aspect ratio of the nanostrip cross section. As the restoring force constant κ goes to zero when the VW becomes unstable upon variation of the nanostrip sizes w and h, one expects large time constants for such walls.

The stationary core displacement is also found from (19) as

$$y_c^* = -\frac{G}{\kappa}u. \qquad (21)$$

Note that, as G can have both signs, VW's with opposite core polarities should display opposite lateral displacements of the core. The increase of y_c^* with u will of course stop at some maximum u_c. According to the linearization performed here, one has

$$u_c = \frac{\kappa w}{2G}, \qquad (22)$$

but deviations from this simple law are anticipated. Investigating them in more detail is not really worthwhile: a full micromagnetic calculation is probably not more difficult but surely more accurate.

Finally, we compute within this model the DW displacement produced by vortex expulsion. From (18) we

obtain by integration

$$[q] = -\frac{G}{\alpha D}\,[\dot{y}_c] = \pm\frac{Gw}{2\alpha D_{xx}}. \tag{23}$$

In order to cast this relation into a more general form, we recall the general definition of the Thiele DW width [18,26]

$$\frac{2}{\Delta_\mathrm{T}} = \frac{1}{S}\int_V \left(\frac{\partial \boldsymbol{m}}{\partial x}\right)^2, \tag{24}$$

where the symbol V below the integral indicates integration over all the nanostrip volume. This DW width applies for any DW type and has been shown to provide the correct understanding of the DW motion velocity in low fields for a VW, for example [18]. In this definition, one should note that Δ_T depends on time. We will thus denote by Δ_T^0 the value for the DW structure at rest with neither field or current applied. As the components of the (opposite of the) Thiele dissipation matrix are defined as [26]

$$D_{ij} = \frac{\mu_0 M_\mathrm{s}}{\gamma_0}\int_V \frac{\partial \boldsymbol{m}}{\partial x_i}\cdot\frac{\partial \boldsymbol{m}}{\partial x_j}, \tag{25}$$

we obtain

$$D_{xx} = (\mu_0 M_\mathrm{s}/\gamma_0) 2S/\Delta_\mathrm{T}, \tag{26}$$

where $S = wh$ is the nanostrip cross section area. Therefore, the DW displacement under vortex expulsion reads finally

$$[q] = \pm\frac{\pi}{2}\frac{\Delta_\mathrm{T}}{\alpha}. \tag{27}$$

This relation is remarkably similar to that obtained for the TW in the 1D model. It can be interpreted as the existence of a wall magnetization angle Φ related to the core position by $\Phi = \pi y_\mathrm{c}/w$. The change of wall angle, that amounted to π for the TW to TW transition, is now $\pi/2$ when the vortex is expulsed and the VW transforms to a TW, an intuitive result. The simple relation (27) can be compared to numerical simulation results. For the 240×10 nm^2 wire, we have at rest $\Delta_\mathrm{T}^0 = 20.1$ nm, and thus compute for $\alpha = 0.02$ a DW displacement under VW to TW conversion equal to 1578 nm, a value extremely close to the numerical result (1600 nm).

For an estimate of the characteristic time τ, we need the restoring force constant κ. As will be discussed later, to every structure is associated a maximum velocity in the absence of current (the Döring maximum velocity). It is related to the maximum core displacement, by relation (21), where $y_\mathrm{c}^* \approx w/2$ and u_c is replaced by v_max. The direct micromagnetic calculation of v_max gives 130 m/s here, from which we obtain $\tau = 12$ ns, a value reasonably close to the numerical value ($\simeq$8 ns).

4 General relations

4.1 Generalized DW magnetization angle

The striking similarity between the TW and VW cases, backed by numerical calculations, is a hint that the relation between DW displacement and change of a 'DW magnetization angle' must be more general. In this section we show that this is indeed the case. The starting point is the LLG equation in presence of a spin-polarized current (1) with $\beta = 0$ for the moment. It can be solved, in terms of the effective field, as

$$\boldsymbol{H}_\mathrm{eff} = \frac{\boldsymbol{m}\times\dot{\boldsymbol{m}}}{\gamma_0} + \frac{\alpha\dot{\boldsymbol{m}}}{\gamma_0} + \frac{u}{\gamma_0}\boldsymbol{m}\times\frac{\partial \boldsymbol{m}}{\partial x} + \lambda\boldsymbol{m}, \tag{28}$$

with λ a number and where for legibility we have abandoned the vectorial notation of the current equivalent velocity. With no applied field, the total DW energy $\mathcal{E}$ is invariant under solid translation along the strip axis x, which is expressed as

$$0 = \frac{\partial \mathcal{E}}{\partial q} = -\mu_0 M_\mathrm{s}\int_V \boldsymbol{H}_\mathrm{eff}\cdot\frac{\partial \boldsymbol{m}}{\partial q} = \mu_0 M_\mathrm{s}\int_V \boldsymbol{H}_\mathrm{eff}\cdot\frac{\partial \boldsymbol{m}}{\partial x}. \tag{29}$$

Replacing now the effective field by expression (28), we remark that the current term disappears (every gradient of $\boldsymbol{m}$ is normal to $\boldsymbol{m}$ as its modulus is constant), leaving

$$\int_V (\boldsymbol{m}\times\dot{\boldsymbol{m}})\cdot\frac{\partial \boldsymbol{m}}{\partial x} + \alpha\int_V \dot{\boldsymbol{m}}\cdot\frac{\partial \boldsymbol{m}}{\partial x} = 0. \tag{30}$$

This relation generalizes equation (3) of the 1D model and (18) of the vortex point core model. Note that, if a field is applied, the DW energy depends on position explicitly according to $\partial\mathcal{E}/\partial q = -2\mu_0 M_\mathrm{s} S H_\mathrm{a}$, so that the right-hand side of (30) will be non zero.

The second term on the left-hand side of (30) computes the projection of $\dot{\boldsymbol{m}}$ on $\partial\boldsymbol{m}/\partial x$, giving a result proportional to DW velocity. We come back to this term in detail later. The first term projects $\dot{\boldsymbol{m}}$ on the other possible direction; it is thus similar to the variation of a DW magnetization angle so that we define

$$\dot{\Phi} = \frac{1}{2S}\int_V \dot{\boldsymbol{m}}\cdot\left(\boldsymbol{m}\times\frac{\partial \boldsymbol{m}}{\partial x}\right). \tag{31}$$

In terms of the magnetization polar and azimuthal angles ϑ and φ this reads

$$\dot{\Phi} = \frac{1}{2S}\int_V \sin\vartheta\left(\frac{\partial\varphi}{\partial t}\frac{\partial\vartheta}{\partial x} - \frac{\partial\vartheta}{\partial t}\frac{\partial\varphi}{\partial x}\right). \tag{32}$$

In the context of bubble domains dynamics, such a quantity was considered earlier by Thiele [36] and Slonczewski [37,38], and called DW momentum as it is conjugated (in Hamilton's sense) to the wall position q (see (35) below).

Note that, if the 1D Bloch wall profile [23] is used to evaluate $\dot{\Phi}$, one finds indeed that the generalized Φ is identical to the angle of the DW magnetization. For a VW, if we assume that the only internal degree of freedom is the core lateral position y_c, then the time derivatives in (32) can be converted into space derivatives, resulting into $\dot{\Phi} = p\pi\dot{y}_\mathrm{c}/w$, a relation already obtained within the vortex point core model. It is however not clear in general that an angle Φ is well defined by the time differential (32). As explained earlier [36], by integration by parts in x and

t, it can be shown that Φ is indeed well defined, and reads for example

$$\Phi = \frac{1}{2S}\int_V \varphi \sin\vartheta \frac{\partial\vartheta}{\partial x} + C^{\rm st}. \tag{33}$$

The difficulty hidden in (33) lies in the continuity of the local angle φ in space and time, a property necessary for the integrations. In the case of bubble domains with Bloch lines in the walls, a procedure involving a discontinuity surface was devised [37]. In our case, such a domain wall model is not general enough. Therefore, we only rely on the proof that, whatever the path, the final angle is the same, and compute Φ by its time derivative that is free of any ambiguity. Although we have not proved it mathematically, we even conjecture that, starting from a given configuration where $\Phi = 0$ is defined, different continuous evolutions leading to the same final structure have values of Φ differing only by a multiple of 2π.

In order to interpret the second term of (30), we use the definition of the Thiele domain wall width (24), and define a general DW velocity $\dot{q}$ as

$$-\frac{\dot{q}}{\Delta_{\rm T}} = \frac{1}{2S}\int_V \dot{\boldsymbol{m}}\cdot\frac{\partial \boldsymbol{m}}{\partial x}. \tag{34}$$

For a rigid DW translation, this definition is correct. It is mathematically different from the operational definition of the DW position extracted from the numerical calculations, namely $q = (1/2S)\int_V m_x$, but numerically the differences are very small. In terms of the above-defined variables, equation (30) is finally written as

$$\dot{\Phi} + \alpha\dot{q}/\Delta_{\rm T} = 0. \tag{35}$$

This relation, identical in form to the well-known first relation (3) of the 1D model, is the central equation of this paper. By integration over time, from $-\infty$ to $+\infty$, we obtain that any change of Φ between initial and final states will be a source of a DW displacement, *whatever the time dependence of the spin-polarized current*. If for simplicity one assumes a constant $\Delta_{\rm T}$, a direct proportionality is obtained. If, going a little further, a 'slave' $\Delta_{\rm T}(\Phi)$ is assumed as in the 1D model, then similarly one gets

$$[q] = -\frac{1}{\alpha}\int_{\Phi_{\rm ini}}^{\Phi_{\rm fin}} \Delta_{\rm T}(\Phi) d\Phi. \tag{36}$$

In any case, relation (35) shows that a DW typical displacement is $\pi\Delta_{\rm T}^0/\alpha$ for a TW flip and $\pi\Delta_{\rm T}^0/(2\alpha)$ for VW to TW conversion, in full agreement with the numerical results. As the integral relation does not depend on the current time dependence, the final state considered may also be reached under current, corresponding to the transient evolution associated with current application. As a result, the independence of the DW transient displacement on the current rise time noted in the numerical simulations (as soon as the final DW structures are the same) is immediately understood.

4.2 DW initial velocity

We now turn to the calculation of the DW velocity just after current onset, in the case of zero risetime. From (1) we have when $\beta = 0$

$$\left.\frac{\partial \boldsymbol{m}}{\partial t}\right|_{0^+} = -\frac{1}{1+\alpha^2}(\boldsymbol{u}\cdot\nabla)\boldsymbol{m}_0 - \frac{\alpha}{1+\alpha^2}\boldsymbol{m}_0\times[(\boldsymbol{u}\cdot\nabla)\boldsymbol{m}_0]. \tag{37}$$

Projecting this derivative on a solid displacement of the DW, we see that the initial velocity is

$$v_0 = \frac{u}{1+\alpha^2}. \tag{38}$$

The other component on the right-hand side of (37) gives, using the definition of the generalized angle Φ (31) and of the Thiele DW width $\Delta_{\rm T}$ (24)

$$\dot{\Phi}_0 = -\frac{\alpha}{1+\alpha^2}\frac{u}{\Delta_{\rm T}^0}. \tag{39}$$

We thus see that the trend apparent in numerical calculations (either as shown above or in the literature [39]), namely $v_0 \approx u$, is very general and structure-independent.

4.3 The maximum velocity of a domain wall

Another general concept valid for any DW type is the existence of a maximum velocity.

From the 1D model for a TW or the point core model for the VW it is well known that DW stationary motion, for example under field, exists only up to the so-called Walker field, with a corresponding maximum velocity. The 1D model discussed above, when restricted to the zero-current case, gives an estimate for this velocity that is the same as (14). Similarly, from our discussion of VW dynamics using the point core model, we can see directly that

$$v_{\rm max} = \frac{\kappa y_{\rm c,max}}{G} \approx \frac{\kappa w}{2G}. \tag{40}$$

The idea of a maximum velocity was introduced very early [31]. Neglecting damping effects as well as energetic terms driving DW motion (damping is small, and both effects have to cancel in terms of total power for a stationary motion), W. Döring showed that stationarily moving structures could be obtained by minimizing a 'kinetic potential', or Lagrangian, composed of the micromagnetic energy density to which a kinetic term is added

$$K = E - \frac{\mu_0 M_{\rm s}}{\gamma_0}\cos\vartheta\,(\boldsymbol{v}\cdot\boldsymbol{\nabla})\varphi. \tag{41}$$

Taking a TW structure, it is obvious that the additional kinetic term in the potential causes a variation of the angle φ at the wall position, in proportion to DW velocity. As φ is fixed by the transverse anisotropy, a solution will be obtained only for low enough velocities.

The notable property of the maximum velocity thus defined is that it does not depend on damping, as readily

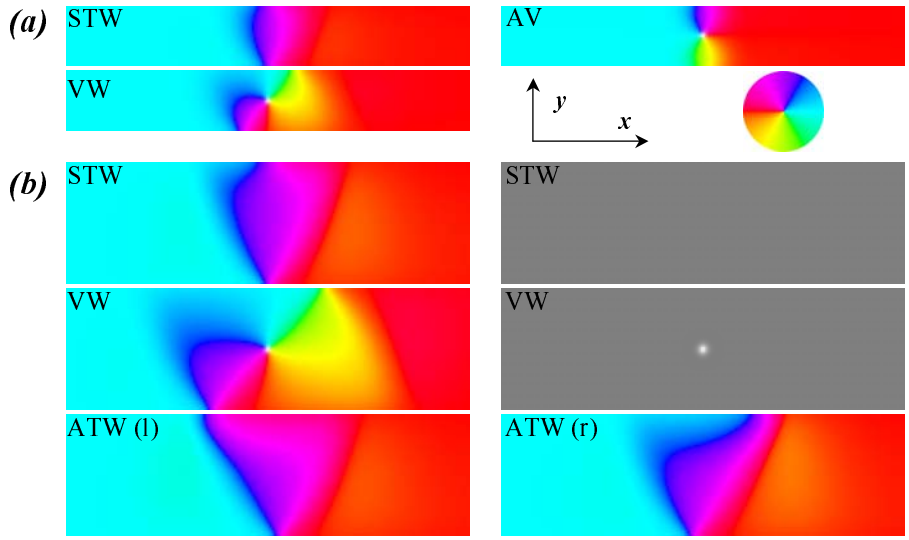

Fig. 6. (Color online) Structures of domain walls in a nanostrip of sizes 120×5 nm^2 (a) and 240×10 nm^2 (b). The equilibrium (stable, metastable or unstable) structures are the symmetric transverse wall (STW), asymmetric transverse wall (ATW) and vortex wall (VW), see the calculated phase diagram [18]. The antivortex structure (AV) that is never stable but appears in dynamics is also shown. Color images represent the in-plane magnetization components, according to the color wheel. The two black and white images (right column, center) display the perpendicular magnetization component, for two of the structures (a non-zero perpendicular magnetization component exists only for VW and AV that have cores with perpendicular magnetization). The ATW is shown in its two variants, with left and right inclination.

seen in the two cases just above. However, as discussed elsewhere [23], the DW structures in stationary motion computed from (41) are independent of α by construction. They are in fact approximations valid for small α, the corrections being of order α^2. For example, from the evolution of DW energy with velocity, Döring introduced the DW mass concept and gave a formula for the Bloch wall, now called the DW mass without damping [38]. But the linearization of the 1D model for small velocities gives a DW mass larger by a factor $1+\alpha^2$. Deviations of order α^2, expected when comparing maximum velocities as seen in dynamic simulations to those obtained from minimization of the kinetic potential, are therefore negligible in practice as $\alpha \simeq 10^{-2}$.

In the presence of a spin-polarized current, the Lagrangian is modified to include the adiabatic term [19,20], so that for stationary motions one has only to replace in (41) the DW velocity $\boldsymbol{v}$ by the relative velocity $\boldsymbol{v} - \boldsymbol{u}$. As a consequence, the range of possible stationary DW velocities in presence of a spin-polarized current becomes $-v_{\max} + u < v < v_{\max} + u$.

4.4 Charts of useful micromagnetic quantities

In order to provide micromagnetic results for practical use, we scan the parameter space of nanostrip sizes, by varying their width w and thickness h. As no anisotropy was assumed in the computations, the physically relevant variables are in fact the scaled values w/Λ and h/Λ, where $\Lambda = \sqrt{2A/\mu_0 M_s^2}$ is the micromagnetic exchange length, whose value is 5 nm for permalloy.

In nanostrips, two main domain wall types exist, the transverse wall (TW) at low w and h, and the vortex wall (VW) at higher w and h [17,18]. The computed stability of these DW structures was confirmed by experiments, provided metastability of the DW structures and influence of defects is considered [40,41] The structures of these walls are displayed in Figure 6 for the nanostrip sizes referred to earlier.

Figure 7 displays data, for both DW types and for the micromagnetic quantities considered before, as a series of contour plots. The plotted quantities should also be scaled with Λ for lengths and $1/(\gamma_0 M_s)$ for time. The value of h is restricted to 20 nm $= 4\Lambda$, as these calculations were performed with a 2D mesh. The thickness was varied in steps of 2 nm maximum and the width in steps of 40 nm maximum. We now discuss these micromagnetic quantities in more detail.

4.4.1 Thiele wall width

A limited chart, restricted to the absolute stability region of each DW type, was published previously [18]. Calculations were performed starting from a VW and a TW, either symmetric (STW) or asymmetric (ATW). They involve a relaxation towards equilibrium followed by the evaluation of the Thiele DW width according to (24). The transition STW-ATW, shown by a dashed line, is second

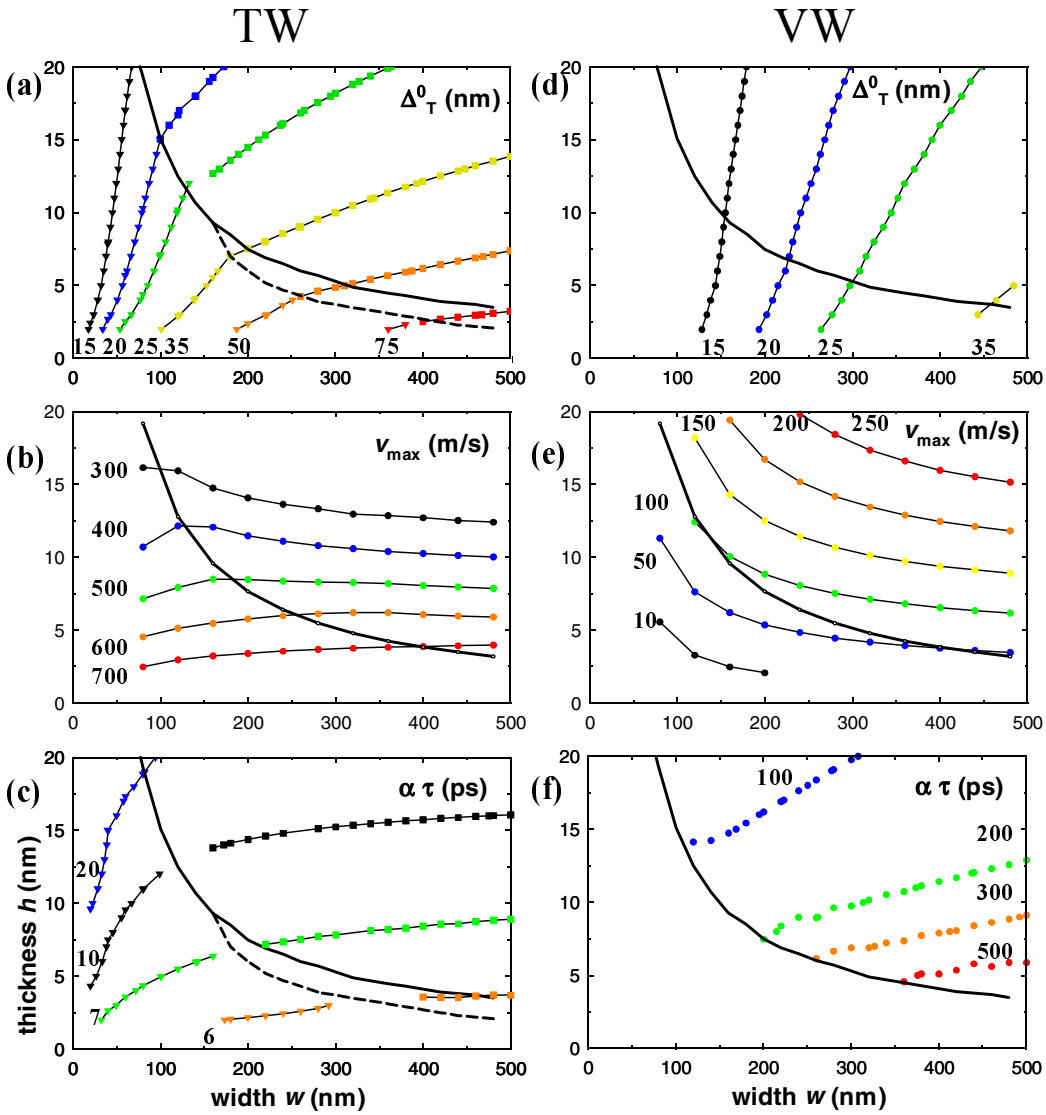

Fig. 7. (Color online) Contour plots, in the (w, h) plane, of 3 micromagnetic quantities useful for the understanding of DW dynamics in nanostrips. Top figures: Thiele DW width Δ_{T}^{0} for the DW at rest. Middle figures: maximum velocity $v_{\max}$. Bottom figures: characteristic time τ of the DW structure relaxation. The left figures refer to transverse walls (either symmetric: triangles or asymmetric: squares, the difference existing only for statics), and the right ones to vortex walls. The equal energy line (TW-VW: continuous line), and the STW-ATW boundary (dashed line) are also drawn. As no anisotropy exists, the numerical values can be adapted to other material parameters using Λ as space and $1/(\gamma_0 M_{\mathrm{s}})$ as time scales.

order (when the nanostrip thickness h is varied, for example) whereas the TW-VW transition, shown by a continuous line, is first order with a large metastability. Therefore, the TW curves correspond to either STW or ATW, depending on position with respect to the second order line. Note that, because of symmetry, it is still possible to converge to a STW within a certain thickness range above the second order transition line. The values thus obtained follow the trend seen in the STW region. This range of thickness was about 10 nm wide with our calculation conditions.

As apparent in the plots (Figs. 7a, 7d), the VW has a smaller Thiele DW width compared to a TW at the same nanostrip dimensions, hence a lower velocity under field and a lower DW displacement under conversion.

4.4.2 Maximum velocity

Data were obtained by minimizing the kinetic potential K for increasing values of the steady-state velocity v, starting from VW and TW. Although the kinetic term (41) requires the (ϑ, φ) representation, the effective field derived from it can be written in vectorial notation [42]. This allows an easy implementation of such calculations in micromagnetic codes.

Notable on the graphs (Figs. 7b, 7e) is first the clear metastability of the DW structures, as both wall types can be moved steadily at $v > 0$ inside the absolute stability region of the other DW type.

The other notable point is the relatively low maximum velocity of the VW, for the usual sizes shown in the diagram, in comparison to the TW. The breakdown mechanism that corresponds to this maximum velocity was discussed before within the point core model: it corresponds to the lateral displacement and expulsion of the vortex core, transforming the VW into a TW. Thus, in some range of parameters, an initial VW can be transformed into a TW under current, the TW then stopping and a DW displacement close to that calculated for a VW to TW transition being measured.

4.4.3 Characteristic time τ

This time τ was calculated from the time evolution of the DW velocity when submitted at $t = 0$ to a small field ($\mu_0 H_x = 0.1$ mT), the damping constant being $\alpha = 0.01$, mostly. Since, from the analytic models and also by comparison to calculations with $\alpha = 0.02$ we find $\tau \propto 1/\alpha$, the value of $\alpha\tau$ is plotted in the chart.

The graphs (Figs. 7c, 7f) show that for the TW the characteristic time constant is small, compared to that of the VW. This is similar to what was seen for the maximum velocity, linked to the motion of the vortex core. As for the maximum velocity also, the time constant depends mainly on the nanostrip thickness, the trends being opposite for the TW and the VW.

In similarity with the data for the Thiele DW width, the relaxation time from STW to ATW could be obtained up to about 10 nm above the second order transition line. This time is of course shorter than the ATW relaxation time, and is not included in the graph.

4.4.4 Use of the charts and comparison to experiments

From the micromagnetic analysis performed here, we obtain two quantities defined for the DW static structure, the Thiele DW width Δ_{T}^0 and the characteristic time τ. In addition, simple formulas exist for the initial DW velocity and wall angle time derivative for a current applied instantaneously, and for the DW mass [34]. Besides, the DW maximum velocity is known. From all these quantities, the prediction of some important aspects of DW propagation under spin-polarized current pulses is possible.

The critical current density required for DW motion, in a perfect sample. In fact, the limit of existence of the zero steady-state velocity under constant current is obtained from the Döring analysis of stationary motion, namely $|u| \leq v_{\max}$. This is the intrinsic threshold current for a perfect sample under a sole adiabatic term [20,19]. From Figure 7, it is apparent that, in these conditions, a VW should move more easily than a TW, as seen experimentally in some cases [8].

However, this qualitative agreement is not quantitative, as the calculated u_{c} values are larger than those measured in experiments, by a factor up to 10. This disagreement can come from the sample heating due to the large current density, and/or from the existence of the non adiabatic torque. Measured temperature rises can reach several hundreds of K [43] and are very dependent on the sample substrate [44], so that the spread of the experimental observations may be caused by the variety of sample architectures. The numerical calculations described above, performed with the room-temperature micromagnetic parameters and discarding the superparamagnetic-type fluctuations of the numerical cell moments, cannot describe the heating effect. However, it can be shown, from a dimensional analysis of (1) where $M_{\mathrm{s}}(T)$ is the scaling parameter, that the scaled spin-transfer torque varies as $1/M_{\mathrm{s}}(T)$. Thus, for permalloy, a temperature rise of 200 K would result into an apparent doubling of the spin-transfer torque. A factor of 10 requires a close approach to T_{c}. The same analysis gives a scaled Langevin field varying as $\sqrt{T/M_{\mathrm{s}}^2(T)}$, so that the same 200 K rise would be equivalent to a Langevin field calculated at $T = 2000$ K without variation of the micromagnetic parameters. The study of fluctuation effects requires a systematic study, dependent on sample dimensions, that is beyond the scope of this paper (see recent theoretical papers on this subject, where extremely high fluctuation temperatures are shown to be required for obtaining measurable effects [45,46]).

On the other hand, the non-adiabatic torque brings the critical current density to zero in a perfect sample, so that a finite critical current density requires a DW pinning potential. In this scheme, the critical current density is dependent on sample quality and cannot be compared to the perfect sample theory discussed here.

The transient DW displacement without DW reversal. When a current is established (slowly or rapidly), we have shown that a DW displacement accumulates that amounts to $[q] \approx u\tau$ ($\alpha \ll 1$). This displacement is also directly related to the change of DW angle. The values are small for a TW but may be large for a VW: with $u = 50$ m/s, $\alpha = 0.01$ and $\alpha\tau = 200$ ps one finds a displacement of 1 μm. For a current pulse, when the DW initial and final states are the same (as monitored by Φ), the total transient DW displacement is zero. However, sample imperfections may hinder vortex core motion, as known to occur in very thin soft films [47] because of the large energy concentrated inside the small vortex core (diameter $\approx 2.6\Lambda$). In such a case, the DW may be out of equilibrium long after the pulse has terminated, as was beautifully shown experimentally for a 500×10 nm^2 sample [8]. In such a situation, the total DW displacement for a series of current pulses up to vortex core expulsion is fixed by theory, and evaluated below.

The DW displacement under structure reversal or transition. The estimate of this total displacement is $[q] = (\pi/2)\Delta_{\mathrm{T}}^0/\alpha$ for a VW-TW transition and $[q] = \pi\Delta_{\mathrm{T}}^0/\alpha$ for a TW reversal. This relation is accurate for the VW case, as the Thiele DW width does not change appreciably when the vortex core displaces laterally. For the TW

however, this width decreases markedly when Φ departs from 0 or π, so that the estimate is an upper limit. The 1D model with the transverse anisotropy ratio κ depicts this behaviour well.

The values of DW displacements upon DW conversion are quite large. For a VW, with $\Delta_{\mathrm{T}}^{0} = 30$ nm and $\alpha = 0.01$ one obtains $[q] = 4.7$ μm. In the case of the 500×10 nm^2 sample quoted above, where DW displacement was seen only when a vortex core was present, the measured total DW displacement up to vortex core expulsion was $\approx$6 μm, close to our estimation. However, this explanation does certainly not apply to all experiments. For example, DW displacements for a 300×27 nm^2 nanostrip [9] as large as 25 μm and linearly varying with pulse duration are clearly of a different origin, even if DW displacement dropped to zero when the vortex core was finally expelled.

5 Conclusion and perspectives

In the framework of purely adiabatic spin transfer and for perfect samples, we have shown that a DW transient displacement occurs when a spin-polarized current in a nanostrip sample is applied. The transient displacement does neither depend on current risetime nor on current pulse length. It is proportional to the change of DW structure. This is a purely gyrotropic effect, similar to the so-called automotion of bubble domains [38].

In order to understand physically this transient displacement, first seen in numerical calculations, we have introduced the concept of a DW angle, a generalization of the intuitive angle of the DW magnetic moment in a TW. It is in fact the adaptation of the wall momentum concept (that was also expressed as an angle), introduced earlier in the context of bubble domains, to the geometry of a nanowire with a single DW. The consideration of this angle allows generalizing the first equation of the 1D DW model, that links the time variation of this angle and of the wall position. From this point of view, it follows that every DW behaves like an effective TW. We note in this respect that an effective 1D model was already applied to VW dynamics with reasonable precision [22,48].

To realize the identification of the type of effective TW, one would need to generalize also the second equation of the 1D model, where the internal energy linked to the variation of the DW angle plays a key role. The vortex point core model, where the core lateral position is directly linked to the DW angle, gives such a potential. Another situation where an effective potential has been introduced is that of the Bloch point wall in nanowires with cross-section of aspect ratio close to unity [23]. A systematic procedure for deriving this internal energy as function of DW angle would therefore be of great interest.

The quantitative evaluation of the transient displacement has shown that it can be quite large, as the small damping amplifies the effect. Thus, experiments should determine when a DW displacement is measured after a current pulse if it depends or not on pulse length, for example. From an other point of view, the transient displacement could also be useful for applications where a DW position change has to be obtained. Finally, the robustness of the conclusions reached here has to be tested against the presence of a non-adiabatic term, and of disorder.

If a non adiabatic term β exists, with $\beta = \alpha$ exactly, then all conclusions reached here should be dismissed as the exact solution of (1) with $\beta = \alpha$ is a rigid displacement of the DW at velocity $v(t) = u(t)$ with the DW structure at rest. More generally, the 1D model shows that the Φ dynamics equation (6) now contains a factor $1-\beta/\alpha$ in front of the u term, so that for $0 < \beta < 2\alpha$ the transient effect will always be reduced. Interestingly, the effect reverses sign when β becomes equal to α. Still more generally, the same procedure by which the angle Φ was introduced for a general DW yields, when the non adiabatic term is included, a generalized equation reading

$$\dot{\Phi} + \alpha\dot{q}/\Delta_{\mathrm{T}} = \beta\frac{u}{\Delta_{\mathrm{T}}}. \tag{42}$$

This equation is identical to (35) if one replaces the DW velocity $\dot{q}$ by $\dot{q} - u\beta/\alpha$. The full analysis of the current effect is therefore more complex, as to the transient effect has to be added the direct displacement caused by the field-like term that appears in (42). The relations can however be worked out very easily in the framework of the 1D model.

The introduction of disorder (DW pinning) is another open subject. A first step would be to introduce a random field H_x with zero mean, function of the DW position only. The statistical physics of this 1D model has been considered already in one case [45], with focus on the 'steady-state' behaviour.

This research was supported by the French Action Concertée Incitative NR 216 PARCOUR, the Programme pluriformations SPINEL of Université Paris-sud, and the european network MRTN-CT-2006-035327 SPINSWITCH. This work was partially performed during a stay of A.T. at the Institute for Chemical Research, Uji, Japan under a JSPS fellowship.

References

1. L. Berger, J. Appl. Phys. **49**, 2156 (1978)
2. L. Berger, J. Appl. Phys. **55**, 1954 (1984)
3. T. Ono, H. Miyajima, K. Shigeto, K. Mibu, N. Hosoito, T. Shinjo, Science **284**, 468 (1999)
4. D. Atkinson, D. Allwood, G. Xiong, M. Cooke, C. Faulkner, R. Cowburn, Nature Mater. **2**, 85 (2003)
5. M. Hayashi, L. Thomas, C. Rettner, R. Moriya, Y. Bazaliy, S. Parkin, Phys. Rev. Lett. **98**, 037204 (2007)
6. N. Vernier, D. Allwood, D. Atkinson, M. Cooke, R. Cowburn, Europhys. Lett. **65**, 526 (2004)
7. A. Yamaguchi, T. Ono, S. Nasu, K. Miyake, K. Mibu, T. Shinjo, Phys. Rev. Lett. **92**, 077205 (2004)
8. M. Kläui, P. Jubert, R. Allenspach, A. Bischof, J. Bland, G. Faini, U. Rüdiger, C. Vaz, L. Vila, C. Vouille, Phys. Rev. Lett. **95**, 026601 (2005)

9. P.O. Jubert, M. Kläui, A. Bischof, U. Rüdiger, R. Allenspach, J. Appl. Phys. **99**, 08G523 (2006)
10. C. Lim, T. Devolder, C. Chappert, J. Grollier, V. Cros, A. Vaurès, A. Fert, G. Faini, Appl. Phys. Lett. **84**, 2820 (2004)
11. J. Miltat, G. Albuquerque, A. Thiaville, *Spin Dynamics in Confined Magnetic Structures I* (Springer, Berlin, 2002), pp. 1–33
12. A. Thiaville, Y. Nakatani, J. Miltat, Y. Suzuki, Europhys. Lett. **69**, 990 (2005)
13. S. Zhang, Z. Li, Phys. Rev. Lett. **93**, 127204 (2004)
14. S. Barnes, S. Maekawa, Phys. Rev. Lett. **95**, 107204 (2005)
15. M. Stiles, W. Saslow, M. Donahue, A. Zangwill, Phys. Rev. B **75**, 214423 (2007)
16. Y. Nakatani, A. Thiaville, J. Miltat, Nature Mater. **2**, 521 (2003)
17. R. McMichael, M. Donahue, IEEE Trans. Magn. **33**, 4167 (1997)
18. Y. Nakatani, A. Thiaville, J. Miltat, J. Magn. Magn. Mater. **290–291**, 750 (2005)
19. A. Thiaville, Y. Nakatani, J. Miltat, N. Vernier, J. Appl. Phys. **95**, 7049 (2004)
20. G. Tatara, H. Kohno, Phys. Rev. Lett. **92**, 086601 (2004)
21. A. Thiaville, J. García, J. Miltat, J. Magn. Magn. Mater. **242–245**, 1061 (2002)
22. L. Thomas, M. Hayashi, X. Jiang, R. Moriya, C. Rettner, S. Parkin, Nature **443**, 197 (2006)
23. A. Thiaville, Y. Nakatani, *Spin Dynamics in Confined Magnetic Structures III* (Springer, Berlin, 2006), pp. 161–206
24. D. Porter, M. Donahue, J. Appl. Phys. **95**, 6729 (2004)
25. J. Shibata (2006), private communication
26. A. Thiele, Phys. Rev. Lett. **30**, 230 (1973)
27. D. Huber, J. Appl. Phys. **53**, 1899 (1982)
28. J. Shibata, Y. Nakatani, G. Tatara, H. Kohno, Y. Otani, Phys. Rev. B **73**, 020403(R) (2006)
29. K.Y. Guslienko, X. Han, D. Keavney, R. Divan, S. Bader, Phys. Rev. Lett. **96**, 067205 (2006)
30. J. He, Z. Li, S. Zhang, J. Appl. Phys. **99**, 08G509 (2006)
31. W. Döring, Z. Naturforschg. **3a**, 373 (1948)
32. J. Slonczewski, *Physics of Magnetic Materials* (World Scientific, Singapore, 1985)
33. G. Wysin, Phys. Rev. B **54**, 15156 (1996)
34. The TW 1D model as well as the VW point core model express the DW Döring mass as $m_{\rm D} = (\mu_0 M_{\rm s}/\gamma_0) 2S\alpha\tau/\Delta_{\rm T}^0$, in terms of the two micromagnetic quantities $\alpha\tau$ and $\Delta_{\rm T}^0$ that we consider in this paper, thus allowing direct evaluation of this mass. This relation shows also that, for the same nanostrip sizes, the VW can bee 100 times heavier than the TW (see Fig. 7).
35. Quantitatively, the values of D_{xx}, D_{yy} and D_{xy}, in units of $(\mu_0 M_{\rm s}/\gamma_0) 2\pi h$, are 3.80, 2.79 and $\pm$ 0.35 for the VW, 1.94, 0.80 and $\pm$ 0.51 for the ATW, and 1.73, 0.40 and 0 for the STW in a 240×10 nm^2 nanostrip, respectively. Thus D_{xx} is dominant for a TW, and $D_{xx} \approx D_{yy}$ dominate for a VW.
36. A. Thiele, J. Appl. Phys. **47**, 2759 (1976)
37. J. Slonczewski, J. Magn. Magn. Mater. **12**, 108 (1979)
38. A. Malozemoff, J. Slonczewski, *Magnetic Domain Walls in Bubble Materials* (Academic Press, New York, 1979)
39. Z. Li, S. Zhang, Phys. Rev. Lett. **92**, 207203 (2004)
40. M. Kläui, C. Vaz, J. Bland, L. Heyderman, F. Nolting, A. Pavlovska, E. Bauer, S. Cherifi, S. Heun, A. Locatelli, Appl. Phys. Lett. **85**, 5637 (2004)
41. M. Laufenberg, D. Backes, W. Bührer, D. Bedau, M. Kläui, U. Rüdiger, C. Vaz, J. Bland, L. Heyderman, F. Nolting et al., Appl. Phys. Lett. **88**, 052507 (2006)
42. K. Yamada, S. Kasai, Y. Nakatani, K. Kobayashi, H. Kohno, A. Thiaville, T. Ono, Nature Mater. **6**, 269 (2007)
43. A. Yamaguchi, S. Nasu, H. Tanigawa, T. Ono, K. Miyake, K. Mibu, T. Shinjo, Appl. Phys. Lett. **86**, 012511 (2005)
44. A. Yamaguchi, K. Yano, H. Tanigawa, S. Kasai, T. Ono, Jpn. J. Appl. Phys. **45**, 3850 (2006)
45. R. Duine, A. Núñez, A. MacDonald, Phys. Rev. Lett. **98**, 056605 (2007)
46. E. Martinez, L. Lopez-Diaz, L. Torres, C. Tristan, O. Alejos, Phys. Rev. B **75**, 174409 (2007)
47. A. Hubert, R. Schäfer, *Magnetic Domains* (Springer Verlag, Berlin, 1998)
48. L. Thomas, M. Hayashi, X. Jiang, R. Moriya, C. Rettner, S. Parkin, Science **315**, 1553 (2007)